Efficient Light Harvesting in Thick Perovskite Solar Cells Processed on Industry-Applicable Random Pyramidal Textures

Ahmed Farag,* Raphael Schmager, Paul Fassl, Philipp Noack, Bianca Wattenberg, Torsten Dippell, and Ulrich W. Paetzold*

ABSTRACT: Light management is key to high-performance solar cells, particularly to monolithic perovskite/Si tandem solar cells and in real field applications. Random pyramidal textures of commercial Si solar cells (height ∼2−5 μm) allow for efficient light harvesting; however, solution processing of conventional perovskite thin films (thickness ∼0.5 μm) over these large textures exhibits bad coverage, resulting in shunting paths. In response to this challenge, we present high-efficiency perovskite solar cells (PSCs) processed on replicated industry-applicable random pyramidal textures with a smaller pyramid size of ∼1−2 μm. As a first step, we develop planar PSCs with close to micrometer thick perovskite absorber layers that maintain efficient charge carrier extraction by using a Lewis base additive and exhibit a power conversion efficiency of up to 18%. Employing these thick films in textured PSCs with inverted pyramids improves the light management as compared to the planar reference, with the AM 1.5G weighted reflectance being reduced from 9.9 to 5.2%. The reduced broadband reflectance in conjunction with enhanced light trapping increases the current generation by 7.7% relative, which corresponds to 87.3% of the maximum attainable short-circuit current density. In addition, we maintain a high fill factor and open-circuit voltage comparable to that of the planar reference PSC despite the increased surface area of the texture. Thereby, our champion textured PSC exhibits a stabilized power output of 18.7% at maximum power point tracking for 5 min. Finally, the textured PSCs also exhibit improved current generation for all angles of incidence, emphasizing their advantages at realistic irradiation conditions and for bifacial applications.

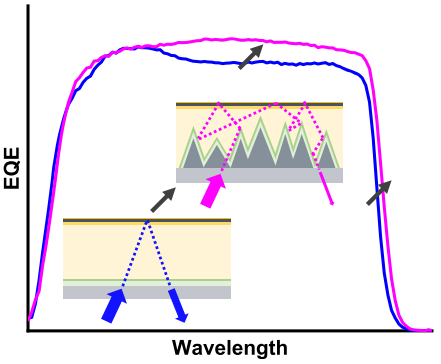

KEYWORDS: *perovskite solar cell, light management, thick perovskite absorber, textured Si, nanoimprint lithography*

INTRODUCTION

In recent years, perovskite/silicon (Si) tandem solar cells, particularly the monolithic two terminal (2T) architecture, have emerged as one of the most promising candidates for low-cost and high-efficiency next generation photovoltaics (PVs) with the potential to surpass the theoretical limit of single-junction solar cells (33%).[1] Recently, Albrecht and co-workers have reported a new record power conversion efficiency (PCE) of 29.80% for 2T perovskite/Si tandem solar cells,[2] just shortly after they achieved a PCE of 29.15%.[3] Both surpass the record PCE of single-junction Si solar cells of 26.7%.[2] The rather straightforward integration of the 2T architecture in conjunction with benefiting from less interlayers that induce parasitic absorption losses gives it an advantage compared to the alternative 4T and 3T architectures.[4−6] However, the 2T architecture requires efficient light management strategies to maximize and match the current generation in both subcells.[4,7,8] Yet, the vast majority of reported high-efficiency 2T perovskite/Si tandem solar cells use front-side polished Si wafers.[9−13] While this approach is compatible with laboratory-scale fabrication, it is industrially not the most favorable option.[14] Moreover, considering that the current generation in monolithic perovskite/Si tandem solar cells is commonly limited by the bottom cell for a wide range of perovskite band gaps,[9,11,15,16] both antireflection and light trapping properties are required to enable current matching.[8,16−20] The pyramidal random textures employed in commercial Si PV are introduced by inexpensive anisotropic wet chemical etching steps. These textures both reduce the reflection losses and enable efficient light trapping, the latter referring to an enhanced optical path length that increases the absorption probability near the band gap.[21−23] Commercial random pyramidal textures for Si PV exhibit a pyramidal texture with a peak to valley distance of ∼5 μm, which results in excellent light management.[17,24−26] However, such large textures are not compatible with solution-processed perovskite thin films that have a typical thickness of ∼0.5 μm.[27] Some earlier studies demonstrated

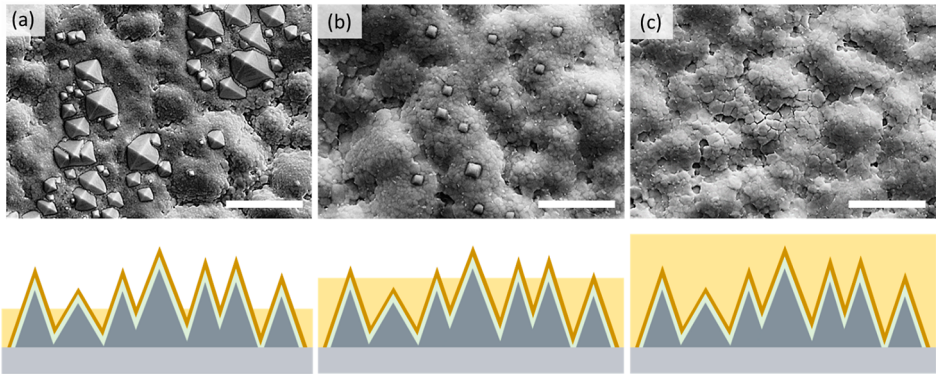

Figure 1. Top view scanning electron microscopy (SEM) images for three perovskite films processed over intermediate-sized textured Si substrates using three different precursor solution molarities (M): (a) 1.2, (b) 1.4, and (c) 1.6 M. The scale bar is 5 μm. The film thickness increases with increase in molarity, resulting in full coverage in the case of 1.6 M, as exemplified in the schematics.

that vacuum deposition[28,29] or a hybrid 2-step process[17,30] allows for conformal coating of these textures, yet the quality of evaporated perovskite solar cells (PSCs) lags behind their solution-processed counterparts.[31,32] Decreasing the pyramidal texture size to ~1−2 μm is an alternative strategy to maintain very good light harvesting, which still allows coating with thick perovskite films.[18,20,33,34] However, spin-coating conventional perovskite thin films over such textures still implies that some of the pyramid tips will protrude from the surface and thereby induce detrimental shunting paths (Figure 1a). While further reducing the texture size would facilitate processing PSCs on top, it easily comes at the cost of increased reflectance due to incomplete texturing.[18,20,33,34] Hence, developing a thick enough perovskite absorber layer that entirely covers such intermediate-sized pyramidal textures has been identified as pivotal for textured perovskite/Si tandem solar cells.[18,33,35−37]

With increasing perovskite layer thickness, efficient charge carrier extraction becomes challenging.[38−41] In fact, most high-quality perovskite thin films reported in the literature exhibit a charge carrier diffusion length of around ~500 nm under solar irradiation conditions, which is too short to allow for efficient charge carrier extraction for film thicknesses of ~1−2 μm.[18,41−44] To address this problem, various strategies for the fabrication of perovskite films have been suggested, including hot casting,[39] vacuum annealing,[45] and solvent retarding.[46] In addition, optimization of the charge transport layers (CTLs) and their interface to the perovskite absorber layer, for example, via surface passivation, has been demonstrated to be critical for efficient charge carrier extraction and thus device performance.[3,18,27,47] Yet, the most popular routes for enhancing the diffusion length within the bulk of the perovskite absorber employ additives in the perovskite precursor solution. Prominent examples are Lewis bases[41,48−50] and Lewis acids,[51] which typically result in a significant increase in the grain size of the perovskite film and a corresponding reduction in trap density, thereby enhancing the charge carrier lifetime and diffusion length. Having a thick, efficient, and stable perovskite absorber over a planar surface provides the capability of investigating the optical gains that come along with processing thick PSCs on intermediate-sized textures.

In this study, we report on the fabrication of highly efficient thick PSCs processed on replicated industry-applicable textured Si wafers with a reduced pyramid size of ~1−2 μm that demonstrate very low reflectance, similar to conventional industrial textured Si wafers. First, we develop thick planar reference PSCs that exhibit efficient charge extraction and PCEs up to 18% by adding the Lewis base urea (CH_4N_2O) to the precursor solution, thereby improving the crystal growth of the close to micrometer thick double-cation perovskite absorber layer ($Cs_{0.17}FA_{0.83}PbI_{2.75}Br_{0.25}$). Second, we investigate the optical gains of processing the developed thick perovskite absorber over the intermediate-sized textures by replicating the Si texture on glass substrates via highly scalable nanoimprint lithography.[52−57] We demonstrate reduced broadband reflectance and improved light trapping near the band gap for textured PSCs compared to the planar reference at standard testing conditions (STC) as well as for angles of incidence (AOI) up to 70°, which could be useful for mono- or bifacial single-junction PSCs in real field applications.[58]

EXPERIMENTAL SECTION

Textured Si Wafers. Appropriate pre-cleaning was done first to remove the saw damage and organic contamination. Then, the anisotropic etching was achieved on n-type, monocrystalline, ⟨100⟩ silicon wafers using alkaline KOH solution and surface activating additive, followed by post-cleaning using HF/HCl to remove the metal residues. More details can be found in ref 59.

Replication. A textured Si wafer was cast into a polydimethylsiloxane (PDMS) mold followed by hardening the PDMS on a hot plate for 4 h at 60 °C. Afterward, it was separated softly from the textured Si wafer and cut to 16 × 16 cm^2 to form a master stamp that fits our glass substrates. OrmoComp resist was deposited over the glass substrate and the stamp was pressed against it and then cured under UV light. The stamp was removed softly after curing to leave the replicated texture on the glass substrate. We note that nanoimprint lithography is a highly scalable process.[53] An illustration of the replication process is shown in Figure S7.

Device Fabrication. *Front Contact.* Patterned indium tin oxide (ITO, 135 nm) as a front contact was sputtered using a Kurt J. Lesker PVD-75 thin-film deposition system. The substrates with the replicated texture were heated up to 235 °C for 15 min in the vacuum chamber before the deposition started and were maintained at this temperature through the whole deposition process. We used a power of 250 W and a gas composition of 96.5% Ar to 3.5% O_2 at a pressure of 0.8 mTorr for 406 s. The sheet resistance of the ITO film was about 25 Ω/cm^2 (depositing at higher temperatures brings the sheet resistance even lower, but the resist will start to exhibit microcracks).

Hole Transport Layer. NiO (15 nm) was sputtered at 150 °C with a power of 100 W from a NiO target with pure Ar at 1 mTorr for 450 s. A 2PACz layer was deposited via spin-coating as reported in ref 60 shortly before the thick perovskite deposition.

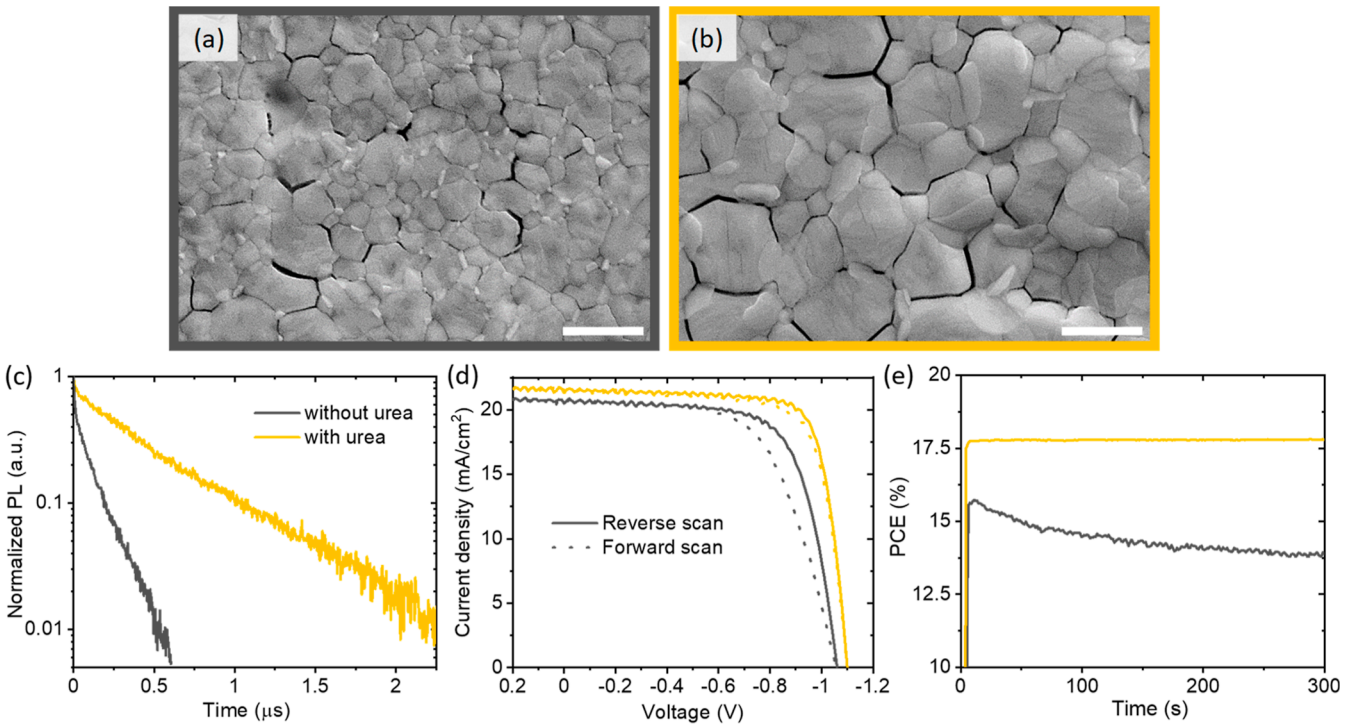

Figure 2. (a,b) Top-view SEM images of a close to micrometer thick perovskite absorber processed over planar glass substrates without (gray) and with (yellow) urea additive, respectively. The scale bar is 1 μm. (c) Time-resolved photoluminescence spectrum for the two perovskite films on glass. (d) *J*–*V* characteristic of the best planar thick PSCs fabricated using the two different perovskite absorbers (statistics of 32 devices are provided in Figure S5a). The solid and dotted lines represent the reverse and forward scan direction, respectively. (e) Corresponding stabilized PCE for the two PSCs under maximum power point tracking (MPPT).

Thick Perovskite. The $Cs_{0.17}FA_{0.83}PbI_{2.75}Br_{0.25}$ precursor solution (1.6 M) was prepared by mixing lead iodide (PbI_2, TCI) and lead bromide ($PbBr_2$, TCI) and dissolving them together in 4:1 *N*,*N*-dimethylformamide (Sigma-Aldrich):dimethyl sulfoxide (Sigma-Aldrich). The solution was heated up for 30 min at 120 °C to dissolve all precursor materials and left to cool down. At room temperature, it was transferred to cesium iodide (Alfa Aesar) and formamidinium iodide (Great Cell Solar) and vigorously agitated until all the powders were dissolved. Note that 10% excess PbI_2 was employed in the precursor solution. Finally, 8 mg/mL of urea (CH_4N_2O, Sigma-Aldrich) was added to the perovskite solution and vigorously agitated before starting the deposition. The solution was spin-coated using a 2-step program: 200 rpm with 300 rpm/s for 2 s followed by 2000 rpm with 2000 rpm/s for 60 s. A solvent-quenching step of 150 μL of ethyl acetate anhydrous (99.8%, $C_4H_8O_2$, Sigma-Aldrich) was dispensed 5 s before the end of the 2nd step. The samples were annealed for 30 min at 100 °C

ETL and Back Electrode. Fullerene (C_{60}, 25 nm thick, Alfa Aesar) and bathocuproine (BCP, 7 nm thick, Luminescence Technology) were thermally evaporated and deposited using OPTIvap evaporation system at a pressure of 5×10^{-7} mbar with a deposition rate of 0.4 and 0.3 A/s, respectively. A 100 nm Ag with 1 A/s was deposited thermally as a back electrode. The active area of our solar cells was 10.5 mm^2, and the band gap of our textured PSCs was ~1.584 eV.

Characterization Methods. *Current Density–Voltage (J–V) Measurements.* The *J*–*V* measurements were performed under AM 1.5G conditions. The stabilized PCE of the cells was determined by the power output at a voltage close to the MPP under continues illumination for 5 min. A shadow mask was used in order to define the active area. Detailed information can be found in ref 6.

For reflectance measurements, we used a PerkinElmer Lambda 1050 spectrometer, and for the angle-dependent reflectance, we used a custom-made holder that allowed us to have a precise angle of incidence (AOI). More information can be found in ref 52.

External Quantum Efficiency Measurements. External quantum efficiency (EQE) measurements were performed using Bentham PVE300 system using an integration time of 500 ms and a chopper frequency of 585 Hz. The angle-dependent EQE measurements were performed using a custom-made holder that allowed us to set the AOI precisely.

RESULTS AND DISCUSSION

Thick Absorber Perovskite Solar Cells. We started with the development of industry-applicable random Si textures with a pyramid size of around 1–2 μm that exhibit low reflectance comparable to conventional Si wafers (see details in the Experimental Section; Figure S1). In order to obtain sufficiently thick perovskite layers for completely covering such intermediate-sized textures, we developed a spin-coating recipe based on the anti-solvent quenching method that uses urea as a Lewis base additive in a double-cation perovskite precursor solution ($Cs_{0.17}FA_{0.83}PbI_{2.75}Br_{0.25}$). As shown in the SEM images in Figure 1, by increasing the molarity of the precursor solution from 1.2 to 1.6 M in steps of 0.2 M and optimizing the parameters for spin-coating and anti-solvent quenching, we obtained full coverage of the textured Si substrates without noticeable pinholes (see details in the Experimental Section). We noted that the thickness on planar substrates increases from ~350 nm when using our base line recipe with 1 M (developed for thin PSCs) to ~1 μm when using 1.6 M with the newly optimized processing parameters as shown in cross-sectional SEM images in Figure S2. By analyzing various cross-sectional SEM images of perovskite films on planar and textured substrates (as in Figure S2b,c), we estimated that the total absorber volume was comparable in both cases. We noted that we achieved a typical PCE of up to ~18.5% for our thin PSCs (without any additive or passivation), as shown in Figure S3. Thick perovskite films as processed here are, however,

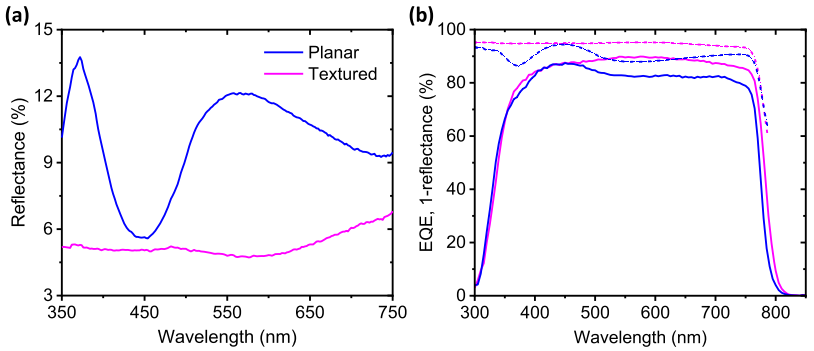

Figure 3. (a) Normal incidence reflection spectrum for the planar reference and textured half-layer stacks [glass/(resist)/ITO/NiO/2PACz/perovskite]. (b) The bold lines refer to the EQE for both the planar reference and textured PSCs with integrated J_{SC}'s of 22.73 and 21.1 mA/cm^2, respectively; the dashed lines represent the 1-reflectance values of the corresponding half-layer stacks.

prone to significant trap state-mediated non-radiative recombination losses, resulting in a low open-circuit voltage (V_{OC}).[40,46] Additionally, the thickness of the absorber layer becomes comparable to or even larger than the charge carrier diffusion length of typical spin-coated perovskite films,[18,40,42−44] or in other words, the charge carriers have a too short lifetime. This could lead to poor charge carrier extraction, thereby negatively affecting both the fill factor (FF) and the short-circuit current density (J_{SC}).[41,61] Growing a perovskite film with large grains that extend throughout the whole film minimizes the density of grain boundaries and has been suggested to result in an enhanced charge carrier mobility, lifetime, and diffusion length.[10,39,49] In that regard, the Lewis base urea has been reported as a promising additive to enhance the grain size and crystallinity of triple-cation,[41] double-cation,[49] and $CH_3NH_3PbI_3$-based perovskite films.[48,50,51,62]

Therefore, we next investigate the impact of urea by comparing perovskite films and PSCs that are processed employing a 1.6 M precursor solution (note that there is a 10% excess of PbI_2) without and with urea additive. Introducing urea to the high molarity perovskite precursor can retard the crystallization and through coordination with PbI_2 results in a damped PbI_2 peak, as shown in the X-ray diffraction (XRD) spectra in Figure S4,[49,50] which enables the perovskite grains to grow larger. The top-view SEM images in Figure 2a,b show that the average domain size increases by a factor of around 3 for the thick perovskite film with urea as compared to the reference. Time-resolved photoluminescence measurements of perovskite films on glass substrates show that the thick perovskite films processed with urea additive possess an increased minority charge carrier lifetime compared to their small grain film counterpart, which we attribute to the reduced density of grain boundaries (see Figure 2c). Together with an improved crystallinity as evident from XRD measurements (Figure S4), this is expected to reduce non-radiative recombination losses and thereby increase the V_{OC} of the PSCs. Indeed, prototype thick PSCs with urea additive comprising the layer stack ITO/2PACz/perovskite/C_{60}/BCP/Ag exhibit an average increase in V_{OC} of ∼50 mV compared to the references, which is accompanied by an average increase in J_{SC} of ∼1 mA/cm^2 and FF from 67 to 77%, indicating more efficient charge carrier extraction (see statistics of 32 devices in Figure S5a). The enhanced J_{sc} for the PSCs with urea is attributed to both an enhanced charge carrier diffusion length (Chen et al.[41] reported an electron diffusion length exceeding 2 μm) and thus improved charge collection as well as reduced parasitic absorption from excess PbI_2 (compare Figure S4) as indicated in Figure S6.[63] The improvements in the individual parameters result in an average PCE of 18% for thick PSCs with urea additive as compared to 14.3% for the references, as derived from the reverse $J-V$ characteristics of 32 devices (Figure S5a). The best thick PSC with urea additive exhibits a PCE of 19% in the reverse $J-V$ scan (on par with thin PSCs without additive, see Figure S3) as compared to 16% for the reference (Figure 2d), which also translates in an enhanced stabilized power output under MPPT for 5 min from 17.8 to 13.9% (Figure 2e). We note that we also fabricated thick planar PSCs with NiO/2PACz as the hole transport layer (HTL; as will be employed for textured PSCs in the following) without and with urea additive, and the trend in device performance is similar to the PSCs employing 2PACz only (see statistics of 26 devices in Figure S5b).

Optics (Textured vs Planar Superstrates). Reflection and parasitic absorption in planar solar cells can result in current density losses of up to 7 mA/cm^2 even in high-efficiency monolithic perovskite/Si tandem solar cells.[56] Applying planar antireflection coatings (ARCs) like MgF_2[10,17,18,57] or LiF[9,11] reduces the reflection losses at the air/front surface interface, but close-to-optimal light incoupling is achieved only by combining textures with ARCs.[8,37,64] With efficient thick PSCs in hand that can fully cover the industry-applicable intermediate-sized textures, the concurrent optical gains are therefore investigated next. To allow for a fair comparison between thick PSCs processed over the textures and planar reference PSCs, we replicate the texture on glass superstrates via nanoimprint lithography. As illustrated in Figure S7, we fabricate a PDMS master stamp from the optimized Si texture of interest and replicate the texture by pressing the stamp against resist deposited on a glass substrate and exposing it to UV light. After replication, half-layer stacks [sputtered ITO (135 nm)/sputtered NiO (15 nm)/2PACz/perovskite] are processed over both the replicated texture and planar substrates in order to investigate and compare the reflection losses. Here, we employ NiO/2PACz as HTL as this combinations ensures a good coverage of the texture without creating detrimental shunting pathways.[65,66] As the resist used in the replication process has almost the same refractive index as glass,[67] illumination from the glass side is feasible and allows for a thorough optical analysis. The reflectance for normal incidence is shown in Figure 3a and highlights that it is lower for the textured stack as compared to the planar reference over the entire spectral range of interest (350−750 nm). While the textured stack exhibits a considerable antireflection effect over the broadband spectrum, the planar stack suffers from higher

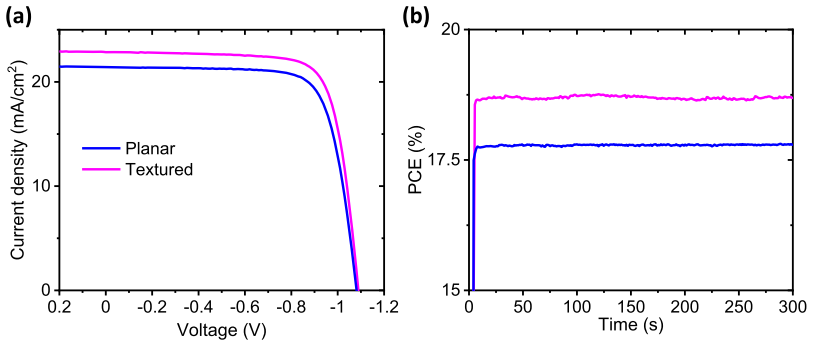

Figure 4. (a) $J-V$ characteristic of the best planar reference and textured PSCs (statistics of 44 devices are provided in Figure S12). (b) Corresponding stabilized PCE under MPPT for 5 min.

reflection losses due to thin-film interference.[29,55] Although the interference pattern in the planar stack approaches the reflectance of the textured stack at around 420 nm, the reflection losses are amplified over the rest of the spectrum, being, for example, 2.5 times higher at around 570 nm. Overall, this correlates to a reduction of the AM 1.5G weighted reflectance from 9.9 to 5.2%. These findings can be attributed to the fact that the intermediate-sized texture enforces multiple incidences on the resist/ITO/NiO/2PACz/perovskite interface even for light rays reflected first.[23,29,55] We note that introducing the same texture at the air/glass interface (the illumination side) can further reduce the reflection losses, as shown in Figure S8. However, improving the light incoupling at this interface is not the focus of the current study, and therefore, no such additional texture is employed in the following.

Next, the impact of the texture on the current generation in the PSCs is investigated (the full device stack and schematics of planar and textured PSCs in Figure S9). As shown in Figure 3b, the EQE is enhanced over the entire spectral range, resulting in an integrated J_{SC} of 22.73 mA/cm^2 as compared to 21.1 mA/cm^2 for the planar reference. In line with the reflectance results discussed above (plotted as 1-reflectance in Figure 3b), the EQE at a wavelength of around 420 nm is very similar for both the textured and reference PSCs, while it is clearly higher for the textured PSCs over the rest of the spectrum. In addition, the EQE close to the band gap is effectively enhanced due to a longer optical path length.[22] Even though for the opaque planar reference PSCs the optical path length is ∼2 times the perovskite absorber layer thickness, the absorption near the band gap is still limited due to the exponential tail of the absorption edge. Introducing the texture increases the optical path length considerably, and consequently, the absorption probability near the band gap is strongly enhanced, as shown in Figure S10. This emphasizes that using the intermediate-sized textures leads to efficient light incoupling into the absorber layer, resulting in optical gains and consequently a higher J_{SC}. As the maximum attainable current density (J_{SQ}) for our perovskite's band gap of ∼1.584 eV (determined from the inflection point of the respective EQE spectrum[68]) is 26.04 mA/cm^2,[1] our approach achieves a J_{SC}/J_{SQ} ratio of 87.3% as compared to 82.6% for the planar reference. We note that we did not employ an additional texture or ARC at the air/glass interface (as discussed above), which would further reduce the reflection losses and increase the J_{SC}/J_{SQ} ratio to among the highest reported.[55] To prove that our concept is also valid for other perovskite compositions that are more suitable for 2T perovskite/Si tandem solar cells, we also processed a thick triple-cation wide band gap perovskite absorber (∼1.67 eV) over the same replicated textures and compared it to a planar reference. As shown in Figure S11, a similar enhancement in the EQE for the textured PSC can be observed. Furthermore, we note that low band gap perovskite absorbers as employed in this work could potentially be used for 3T perovskite/Si tandem solar cells in which current matching is not a requirement.[4,5]

Performance of Textured Thick Perovskite Solar Cells for Variable Angles of Incidence. Having demonstrated that textured PSCs benefit from high current densities, we report next on the overall device performance. Figure 4a shows the $J-V$ characteristic of the champion textured and planar reference PSCs from the same batch (statistics of 44 devices are provided in Figure S12). Next to the apparent increase in J_{SC}, it is noteworthy that a comparable V_{OC} and FF are achieved for the textured PSC compared to the planar reference. Apparently, the HTL/perovskite interface must be of high quality as the surface area of the textured PSC is strongly enhanced, but still no significant non-radiative recombination losses appear (cf. high V_{OC}), which we attribute to a good coverage of the self-assembled monolayer 2PACz on NiO,[65,66] together with the high optoelectronic quality of the 2PACz/perovskite interface.[27,55,60,65,66] Thereby, the PCE is consistently enhanced from 17.8 to 18.7% also for several minutes of MPPT (Figure 4b). The enhancement in performance was reproduced in a number of devices, as shown in Figure S12. We would like to note that we also successfully fabricated highly efficient semitransparent PSCs directly on top of textured Si substrates that exhibit PCEs of 16.5 and 15.8% for a band gap of ∼1.6 and ∼1.67 eV, respectively (see Figure S13). This stresses the potential of our spin-coating approach for 2T or 3T perovskite/Si tandem solar cells with intermediate-sized textures, which will be the focus of a future work.

As a side note, we want to point out that the textured PSCs reported in this work required the development of a dedicated ITO recipe. While our conventional sputtered ITO front electrode exhibits a sheet resistance > 65 Ω/cm^2 if sputtered on top of textured superstrates, the adapted new sputtering recipe allowed obtaining high-quality ITO films with sheet resistance < 20 Ω/cm^2 even over the industry-applicable textures. More details on the device fabrication and the ITO sputtering process can be found in the Experimental Section.

Having demonstrated superior light harvesting in thick PSCs processed over the micrometer-sized industry-applicable textures at STC, we examine the angular dependence of reflectance and J_{SC} in these devices. Under realistic irradiation

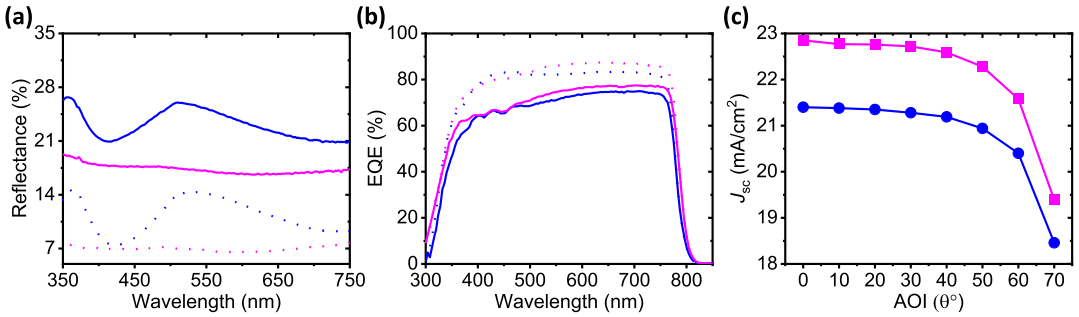

Figure 5. (a) Reflection spectra for the planar reference (blue) and textured (pink) stack at AOI θ = 30° (dotted) and θ = 70° (solid). (b) Corresponding external quantum efficiency at AOI θ = 30° and θ = 70°; the full data set is presented in Figure S14. (c) Corresponding integrated short-circuit current density (J_{SC}) for each EQE value per each AOI (from normal incidence till θ = 70° in 10° steps).

conditions as well as for backside illumination in bifacial single-junction PSCs,[7,37,58,64] the incident light is barely normal to the solar cell's plane, which leads to considerable angular reflection losses for certain device architectures.[64,69,70] The industry-applicable textures introduced in this study in the superstrate of the textured PSCs facilitate light incoupling also for AOI θ > 0°. The texture enforces incident light to impinge multiple times on the interface of the resin/solar cell and thereby vastly reduces the reflection losses.[4,57,64] As a consequence, PSCs fabricated over the industry-applicable textured substrates tolerate a large range of incident angles. This is exemplarily shown in Figure 5a, where the reflectance of the planar reference is compared to the reflectance of the textured PSCs at 30 and 70° AOI. It should be noted that the interference pattern of the planar stack is blue shifted and peaks at 510 nm with a reflectance value of 26% for 70° AOI, while the textured stack exhibits a reflectance of only 17.4% at the same wavelength.

Finally, the angle dependence of current generation in the textured PSCs is compared to the planar reference. In full agreement with the angle-dependent reflectance data, the EQE is in favor of the textured stack at both 30 and 70° AOI, as shown in Figure 5b (the full data set is provided in Figure S14).[4] The integrated J_{SC} values for various AOIs is shown in Figure 5c, emphasizing that the improved light-harvesting characteristics of our textured PSCs is present for all AOI. Consequently, our approach could be useful for realistic irradiation scenarios and bifacial applications.[7,37,58,64]

CONCLUSIONS

In this study, we present close to micrometer thick PSCs processed over replicated industry-applicable random pyramidal textures for efficient light harvesting. Our texture exhibits a pyramid size of ∼1−2 μm and maintains efficient broadband light incoupling as well as excellent light trapping close to the perovskite band gap. To achieve sufficiently long diffusion length and efficient charge carrier extraction in our thick perovskite absorber layers, we use urea as a Lewis base additive to improve the crystallization and in turn the grain size and film quality of the thick perovskite films. Having first optimized the thick absorber layer over a planar stack, thick PSCs processed over industry-applicable random pyramid textures are demonstrated. The textures were replicated on glass substrates using highly scalable nanoimprint lithography. The textured PSCs exhibit reduced reflection losses compared to the planar reference over the broadband spectrum both in normal incidence and for AOI up to 70°, leading to vastly improved light harvesting. The optical gains resulted in a respectable J_{SC} that relates to ∼87.3% of the theoretical limit, which is 4.7% higher in absolute terms compared to the planar reference. By having an FF and V_{OC} comparable to that of the planar reference, the impact of light management using our approach reflected on the PCE of the textured PSCs with a stabilized power output of up to 18.7%. In addition to the potential application for textured 2T and 3T perovskite/Si tandem solar cells, our approach could be beneficial for mono- or bifacial single-junction PSCs in real field applications.

AUTHOR INFORMATION

Corresponding Authors

Ahmed Farag − *Institute of Microstructure Technology, Karlsruhe Institute of Technology (KIT), Eggenstein-Leopoldshafen 76344, Germany; Light Technology Institute, Karlsruhe Institute of Technology (KIT), Karlsruhe 76131, Germany*; Email: ahmed.farag@kit.edu

Ulrich W. Paetzold − *Institute of Microstructure Technology, Karlsruhe Institute of Technology (KIT), Eggenstein-Leopoldshafen 76344, Germany; Light Technology Institute, Karlsruhe Institute of Technology (KIT), Karlsruhe 76131, Germany*; orcid.org/0000-0002-1557-8361; Email: ulrich.paetzold@kit.edu

Authors

Raphael Schmager − *Institute of Microstructure Technology, Karlsruhe Institute of Technology (KIT), Eggenstein-Leopoldshafen 76344, Germany*; orcid.org/0000-0003-2467-6171

Paul Fassl − *Institute of Microstructure Technology, Karlsruhe Institute of Technology (KIT), Eggenstein-Leopoldshafen 76344, Germany; Light Technology Institute, Karlsruhe Institute of Technology (KIT), Karlsruhe 76131, Germany;* orcid.org/0000-0002-9604-3405

Philipp Noack − *Singulus Technologies AG, Kahl/Main D-63796, Germany*

Bianca Wattenberg − *Singulus Technologies AG, Kahl/Main D-63796, Germany*

Torsten Dippell − *Singulus Technologies AG, Kahl/Main D-63796, Germany*

Notes

The authors declare no competing financial interest.

ACKNOWLEDGMENTS

The authors gratefully acknowledge financial support by the Initiating and Networking funding of the Helmholtz Association [HYIG of U.W.P. (VHNG-1148)], the Helmholtz Energy Materials Foundry (HEMF), PEROSEED (ZT0024), the German Federal Ministry for Economic Affairs (BMWi) through project 27Plus6 (03EE1056B) as well as project CAPITANO (03EE1038B), and the Karlsruhe School of Optics and Photonics (KSOP). The authors acknowledge the Helmholtz Association (program-oriented funding IV, Materials and Technologies for the Energy Transition, Topic 1: Photovoltaics and Wind Energy, Code: 38.01.02).

REFERENCES

(1) Shockley, W.; Queisser, H. J. Detailed Balance Limit of Efficiency of P-n Junction Solar Cells. *J. Appl. Phys.* **1961**, *32*, 510−519.

(2) NREL Best Research-Cell Efficiency Chart. https://www.nrel.gov/pv/cell-efficiency.html (accessed on March 15, 2022).

(3) Al-Ashouri, A.; Köhnen, E.; Li, B.; Magomedov, A.; Hempel, H.; Caprioglio, P.; Márquez, J. A.; Morales Vilches, A. B.; Kasparavicius, E.; Smith, J. A.; Phung, N.; Menzel, D.; Grischek, M.; Kegelmann, L.; Skroblin, D.; Gollwitzer, C.; Malinauskas, T.; Jošt, M.; Matič, G.; Rech, B.; Schlatmann, R.; Topič, M.; Korte, L.; Abate, A.; Stannowski, B.; Neher, D.; Stolterfoht, M.; Unold, T.; Getautis, V.; Albrecht, S. Monolithic Perovskite/Silicon Tandem Solar Cell with >29% Efficiency by Enhanced Hole Extraction. *Science* **2020**, *370*, 1300−1309.

(4) Gota, F.; Langenhorst, M.; Schmager, R.; Lehr, J.; Paetzold, U. W. Energy Yield Advantages of Three-Terminal Perovskite-Silicon Tandem Photovoltaics. *Joule* **2020**, *4*, 2387−2403.

(5) Tockhorn, P.; Wagner, P.; Kegelmann, L.; Stang, J.-C.; Mews, M.; Albrecht, S.; Korte, L. Three-Terminal Perovskite/Silicon Tandem Solar Cells with Top and Interdigitated Rear Contacts. *ACS Appl. Energy Mater.* **2020**, *3*, 1381−1392.

(6) Gharibzadeh, S.; Hossain, I. M.; Fassl, P.; Nejand, B. A.; Abzieher, T.; Schultes, M.; Ahlswede, E.; Jackson, P.; Powalla, M.; Schäfer, S.; Rienäcker, M.; Wietler, T.; Peibst, R.; Lemmer, U.; Richards, B. S.; Paetzold, U. W. 2D/3D Heterostructure for Semitransparent Perovskite Solar Cells with Engineered Bandgap Enables Efficiencies Exceeding 25% in Four-Terminal Tandems with Silicon and CIGS. *Adv. Funct. Mater.* **2020**, *30*, 1909919.

(7) Singh, M.; Santbergen, R.; Syifai, I.; Weeber, A.; Zeman, M.; Isabella, O. Comparing Optical Performance of a Wide Range of Perovskite/Silicon Tandem Architectures under Real-World Conditions. *Nanophotonics* **2021**, *10*, 2043−2057.

(8) Jacobs, D. A.; Langenhorst, M.; Sahli, F.; Richards, B. S.; White, T. P.; Ballif, C.; Catchpole, K. R.; Paetzold, U. W. Light Management: A Key Concept in High-Efficiency Perovskite/Silicon Tandem Photovoltaics. *J. Phys. Chem. Lett.* **2019**, *10*, 3159−3170.

(9) Bush, K. A.; Palmstrom, A. F.; Yu, Z. J.; Boccard, M.; Cheacharoen, R.; Mailoa, J. P.; McMeekin, D. P.; Hoye, R. L. Z.; Bailie, C. D.; Leijtens, T.; Peters, I. M.; Minichetti, M. C.; Rolston, N.; Prasanna, R.; Sofia, S.; Harwood, D.; Ma, W.; Moghadam, F.; Snaith, H. J.; Buonassisi, T.; Holman, Z. C.; Bent, S. F.; McGehee, M. D. 23.6%-Efficient Monolithic Perovskite/Silicon Tandem Solar Cells with Improved Stability. *Nat. Energy* **2017**, *2*, 17009.

(10) Chen, B.; Yu, Z.; Liu, K.; Zheng, X.; Liu, Y.; Shi, J.; Spronk, D.; Rudd, P. N.; Holman, Z.; Huang, J. Grain Engineering for Perovskite/Silicon Monolithic Tandem Solar Cells with Efficiency of 25.4%. *Joule* **2019**, *3*, 177−190.

(11) Köhnen, E.; Jošt, M.; Morales-Vilches, A. B.; Tockhorn, P.; Al-Ashouri, A.; Macco, B.; Kegelmann, L.; Korte, L.; Rech, B.; Schlatmann, R.; Stannowski, B.; Albrecht, S. Highly Efficient Monolithic Perovskite Silicon Tandem Solar Cells: Analyzing the Influence of Current Mismatch on Device Performance. *Sustain. Energy Fuels* **2019**, *3*, 1995−2005.

(12) Xu, J.; Boyd, C. C.; Yu, Z. J.; Palmstrom, A. F.; Witter, D. J.; Larson, B. W.; France, R. M.; Werner, J.; Harvey, S. P.; Wolf, E. J.; Weigand, W.; Manzoor, S.; van Hest, M. F. A. M.; Berry, J. J.; Luther, J. M.; Holman, Z. C.; McGehee, M. D. Triple-halide wide-band gap perovskites with suppressed phase segregation for efficient tandems. *Science* **2020**, *367*, 1097−1104.

(13) Kim, D.; Jung, H. J.; Park, I. J.; Larson, B. W.; Dunfield, S. P.; Xiao, C.; Kim, J.; Tong, J.; Boonmongkolras, P.; Ji, S. G.; Zhang, F.; Pae, S. R.; Kim, M.; Kang, S. B.; Dravid, V.; Berry, J. J.; Kim, J. Y.; Zhu, K.; Kim, D. H.; Shin, B. Efficient, Stable Silicon Tandem Cells Enabled by Anion-Engineered Wide-Bandgap Perovskites. *Science* **2020**, *368*, 155.

(14) Werner, J.; Niesen, B.; Ballif, C. Perovskite/Silicon Tandem Solar Cells: Marriage of Convenience or True Love Story? - An Overview. *Adv. Mater. Interfaces* **2018**, *5*, 1700731.

(15) Shen, H.; Omelchenko, S. T.; Jacobs, D. A.; Yalamanchili, S.; Wan, Y.; Yan, D.; Phang, P.; Duong, T.; Wu, Y.; Yin, Y.; Samundsett, C.; Peng, J.; Wu, N.; White, T. P.; Andersson, G. G.; Lewis, N. S.; Catchpole, K. R. In Situ Recombination Junction between P-Si and TiO 2 Enables High-Efficiency Monolithic Perovskite/Si Tandem Cells. *Sci. Adv.* **2018**, *4*, No. eaau9711.

(16) Xu, Q.; Zhao, Y.; Zhang, X. Light Management in Monolithic Perovskite/Silicon Tandem Solar Cells. *Sol. RRL* **2020**, *4*, 1900206.

(17) Sahli, F.; Werner, J.; Kamino, B. A.; Bräuninger, M.; Monnard, R.; Paviet-Salomon, B.; Barraud, L.; Ding, L.; Diaz Leon, J. J.; Sacchetto, D.; Cattaneo, G.; Despeisse, M.; Boccard, M.; Nicolay, S.; Jeangros, Q.; Niesen, B.; Ballif, C. Fully Textured Monolithic Perovskite/Silicon Tandem Solar Cells with 25.2% Power Conversion Efficiency. *Nat. Mater.* **2018**, *17*, 820−826.

(18) Hou, Y.; Aydin, E.; De Bastiani, M.; Xiao, C.; Isikgor, F. H.; Xue, D.-J.; Chen, B.; Chen, H.; Bahrami, B.; Chowdhury, A. H.; Johnston, A.; Baek, S.-W.; Huang, Z.; Wei, M.; Dong, Y.; Troughton, J.; Jalmood, R.; Mirabelli, A. J.; Allen, T. G.; Van Kerschaver, E.; Saidaminov, M. I.; Baran, D.; Qiao, Q.; Zhu, K.; De Wolf, S.; Sargent, E. H. Efficient Tandem Solar Cells with Solution-Processed Perovskite on Textured Crystalline Silicon. *Science* **2020**, *367*, 1135−1140.

(19) De Bastiani, M.; Mirabelli, A. J.; Hou, Y.; Gota, F.; Aydin, E.; Allen, T. G.; Troughton, J.; Subbiah, A. S.; Isikgor, F. H.; Liu, J.; Xu, L.; Chen, B.; Van Kerschaver, E.; Baran, D.; Fraboni, B.; Salvador, M. F.; Paetzold, U. W.; Sargent, E. H.; De Wolf, S. Efficient Bifacial Monolithic Perovskite/Silicon Tandem Solar Cells via Bandgap Engineering. *Nat. Energy* **2021**, *6*, 167−175.

(20) Subhan, F. E.; Khan, A. D.; Khan, A. D.; Ullah, N.; Imran, M.; Noman, M. Optical optimization of double-side-textured monolithic perovskite-silicon tandem solar cells for improved light management. *RSC Adv.* **2020**, *10*, 26631−26638.

(21) Hua, X.-S.; Zhang, Y.-J.; Wang, H.-W. The Effect of Texture Unit Shape on Silicon Surface on the Absorption Properties. *Sol. Energy Mater. Sol. Cells* **2010**, *94*, 258−262.

(22) Yablonovitch, E. Statistical Ray Optics. *J. Opt. Soc. Am.* **1982**, *72*, 899.
(23) Jošt, M.; Köhnen, E.; Morales-Vilches, A. B.; Lipovšek, B.; Jäger, K.; Macco, B.; Al-Ashouri, A.; Krč, J.; Korte, L.; Rech, B.; Schlatmann, R.; Topič, M.; Stannowski, B.; Albrecht, S. Textured Interfaces in Monolithic Perovskite/Silicon Tandem Solar Cells: Advanced Light Management for Improved Efficiency and Energy Yield. *Energy Environ. Sci.* **2018**, *11*, 3511−3523.
(24) Basu, P. K.; Khanna, A.; Hameiri, Z. The Effect of Front Pyramid Heights on the Efficiency of Homogeneously Textured Inline-Diffused Screen-Printed Monocrystalline Silicon Wafer Solar Cells. *Renewable Energy* **2015**, *78*, 590−598.
(25) Basu, P. K.; Sarangi, D.; Shetty, K. D.; Boreland, M. B. Liquid Silicate Additive for Alkaline Texturing of Mono-Si Wafers to Improve Process Bath Lifetime and Reduce IPA Consumption. *Sol. Energy Mater. Sol. Cells* **2013**, *113*, 37−43.
(26) Baker-Finch, S. C.; McIntosh, K. R. Reflection Distributions of Textured Monocrystalline Silicon: Implications for Silicon Solar Cells. *Prog. Photovoltaics Res. Appl.* **2012**, *21*, a−n.
(27) Gharibzadeh, S.; Fassl, P.; Hossain, I. M.; Rohrbeck, P.; Frericks, M.; Schmidt, M.; Duong, T.; Khan, M. R.; Abzieher, T.; Nejand, B. A.; Schackmar, F.; Almora, O.; Feeney, T.; Singh, R.; Fuchs, D.; Lemmer, U.; Hofmann, J. P.; Weber, S. A. L.; Paetzold, U. W. Two Birds with One Stone: Dual Grain-Boundary and Interface Passivation Enables >22% Efficient Inverted Methylammonium-Free Perovskite Solar Cells. *Energy Environ. Sci.* **2021**, *14*, 5875−5893.
(28) Hamada, K.; Yonezawa, K.; Yamamoto, K.; Taima, T.; Hayase, S.; Ooyagi, N.; Yamamoto, Y.; Ohdaira, K. Vacuum Deposition of CsPbI3 Layers on Textured Si for Perovskite/Si Tandem Solar Cells. *Jpn. J. Appl. Phys.* **2019**, *58*, SBBF06.
(29) Gil-Escrig, L.; Roß, M.; Sutter, J.; Al-Ashouri, A.; Becker, C.; Albrecht, S. Fully Vacuum-Processed Perovskite Solar Cells on Pyramidal Microtextures. *Sol. RRL* **2021**, *5*, 2000553.
(30) Lee, S.-W.; Bae, S.; Hwang, J.-K.; Lee, W.; Lee, S.; Hyun, J. Y.; Cho, K.; Kim, S.; Heinz, F. D.; Bin Choi, S.; Choi, D.; Kang, D.; Yang, J.; Jeong, S.; Park, S. J.; Schubert, M. C.; Glunz, S.; Kim, W. M.; Kang, Y.; Lee, H.-S.; Kim, D. Perovskites Fabricated on Textured Silicon Surfaces for Tandem Solar Cells. *Commun. Chem.* **2020**, *3*, 37.
(31) Vaynzof, Y. The Future of Perovskite Photovoltaics-Thermal Evaporation or Solution Processing? *Adv. Energy Mater.* **2020**, *10*, 2003073.
(32) Abzieher, T.; Feeney, T.; Schackmar, F.; Donie, Y. J.; Hossain, I. M.; Schwenzer, J. A.; Hellmann, T.; Mayer, T.; Powalla, M.; Paetzold, U. W. From Groundwork to Efficient Solar Cells: On the Importance of the Substrate Material in Co-Evaporated Perovskite Solar Cells. *Adv. Funct. Mater.* **2021**, *31*, 2104482.
(33) Chen, B.; Yu, Z. J.; Manzoor, S.; Wang, S.; Weigand, W.; Yu, Z.; Yang, G.; Ni, Z.; Dai, X.; Holman, Z. C.; Huang, J. Blade-Coated Perovskites on Textured Silicon for 26%-Efficient Monolithic Perovskite/Silicon Tandem Solar Cells. *Joule* **2020**, *4*, 850−864.
(34) Alasfour, A.; Yu, Z. J.; Weigand, W.; Quispe, D.; Holman, Z. C. Sub-Micrometer Random-Pyramid Texturing of Silicon Solar Wafers with Excellent Surface Passivation and Low Reflectance. *Sol. Energy Mater. Sol. Cells* **2020**, *218*, 110761.
(35) Aydin, E.; Liu, J.; Ugur, E.; Azmi, R.; Harrison, G. T.; Hou, Y.; Chen, B.; Zhumagali, S.; De Bastiani, M.; Wang, M.; Raja, W.; Allen, T. G.; Rehman, A. u.; Subbiah, A. S.; Babics, M.; Babayigit, A.; Isikgor, F. H.; Wang, K.; Van Kerschaver, E.; Tsetseris, L.; Sargent, E. H.; Laquai, F.; De Wolf, S. Ligand-bridged charge extraction and enhanced quantum efficiency enable efficient n-i-p perovskite/silicon tandem solar cells. *Energy Environ. Sci.* **2021**, *14*, 4377−4390.
(36) Wang, J.; Gao, C.; Wang, X.; Wang, Y.; Cheng, Z.; Liu, H.; Shen, W. Simple Solution-Processed Approach for Nanoscale Coverage of Perovskite on Textured Silicon Surface Enabling Highly Efficient Perovskite/Si Tandem Solar Cells. *Energy Technol.* **2021**, *9*, 2000778.
(37) Lehr, J.; Langenhorst, M.; Schmager, R.; Gota, F.; Kirner, S.; Lemmer, U.; Richards, B. S.; Case, C.; Paetzold, U. W. Energy Yield of Bifacial Textured Perovskite/Silicon Tandem Photovoltaic Modules. *Sol. Energy Mater. Sol. Cells* **2020**, *208*, 110367.
(38) Wang, K.; Liu, C.; Du, P.; Chen, L.; Zhu, J.; Karim, A.; Gong, X. Efficiencies of perovskite hybrid solar cells influenced by film thickness and morphology of CH3NH3PbI3−xClx layer. *Org. Electron.* **2015**, *21*, 19−26.
(39) Chen, J.; Zuo, L.; Zhang, Y.; Lian, X.; Fu, W.; Yan, J.; Li, J.; Wu, G.; Li, C.-Z.; Chen, H. High-Performance Thickness Insensitive Perovskite Solar Cells with Enhanced Moisture Stability. *Adv. Energy Mater.* **2018**, *8*, 1800438.
(40) Rai, M.; Wong, L. H.; Etgar, L. Effect of Perovskite Thickness on Electroluminescence and Solar Cell Conversion Efficiency. *J. Phys. Chem. Lett.* **2020**, *11*, 8189−8194.
(41) Chen, B.; Baek, S.-W.; Hou, Y.; Aydin, E.; De Bastiani, M.; Scheffel, B.; Proppe, A.; Huang, Z.; Wei, M.; Wang, Y.-K.; Jung, E.-H.; Allen, T. G.; Van Kerschaver, E.; García de Arquer, F. P.; Saidaminov, M. I.; Hoogland, S.; De Wolf, S.; Sargent, E. H. Enhanced Optical Path and Electron Diffusion Length Enable High-Efficiency Perovskite Tandems. *Nat. Commun.* **2020**, *11*, 1257.
(42) Sandberg, O. J.; Kurpiers, J.; Stolterfoht, M.; Neher, D.; Meredith, P.; Shoaee, S.; Armin, A. On the Question of the Need for a Built-In Potential in Perovskite Solar Cells. *Adv. Mater. Interfaces* **2020**, *7*, 2000041.
(43) Bahrami, B.; Chowdhury, A. H.; Gurung, A.; Mabrouk, S.; Reza, K. M.; Rahman, S. I.; Pathak, R.; Qiao, Q. Nanoscale Spatial Mapping of Charge Carrier Dynamics in Perovskite Solar Cells. *Nano Today* **2020**, *33*, 100874.
(44) Bercegol, A.; Ory, D.; Suchet, D.; Cacovich, S.; Fournier, O.; Rousset, J.; Lombez, L. Quantitative Optical Assessment of Photonic and Electronic Properties in Halide Perovskite. *Nat. Commun.* **2019**, *10*, 1586.
(45) Eggers, H.; Schackmar, F.; Abzieher, T.; Sun, Q.; Lemmer, U.; Vaynzof, Y.; Richards, B. S.; Hernandez-Sosa, G.; Paetzold, U. W. Inkjet-Printed Micrometer-Thick Perovskite Solar Cells with Large Columnar Grains. *Adv. Energy Mater.* **2020**, *10*, 1903184.
(46) Yuan, Z.; Yang, Y.; Wu, Z.; Bai, S.; Xu, W.; Song, T.; Gao, X.; Gao, F.; Sun, B. Approximately 800-Nm-Thick Pinhole-Free Perovskite Films via Facile Solvent Retarding Process for Efficient Planar Solar Cells. *ACS Appl. Mater. Interfaces* **2016**, *8*, 34446−34454.
(47) Yan, K.; Chen, J.; Ju, H.; Ding, F.; Chen, H.; Li, C.-Z. Achieving High-Performance Thick-Film Perovskite Solar Cells with Electron Transporting Bingel Fullerenes. *J. Mater. Chem. A* **2018**, *6*, 15495−15503.
(48) Hsieh, C.-M.; Liao, Y.-S.; Lin, Y.-R.; Chen, C.-P.; Tsai, C.-M.; Wei-Guang Diau, E.; Chuang, S.-C. Low-Temperature, Simple and Efficient Preparation of Perovskite Solar Cells Using Lewis Bases Urea and Thiourea as Additives: Stimulating Large Grain Growth and Providing a PCE up to 18.8. *RSC Adv.* **2018**, *8*, 19610−19615.
(49) Zhu, L.; Xu, Y.; Zhang, P.; Shi, J.; Zhao, Y.; Zhang, H.; Wu, J.; Luo, Y.; Li, D.; Meng, Q. Investigation on the Role of Lewis Bases in the Ripening Process of Perovskite Films for Highly Efficient Perovskite Solar Cells. *J. Mater. Chem. A* **2017**, *5*, 20874−20881.
(50) Han, L.; Cong, S.; Yang, H.; Lou, Y.; Wang, H.; Huang, J.; Zhu, J.; Wu, Y.; Chen, Q.; Zhang, B.; Zhang, L.; Zou, G. Environmental-Friendly Urea Additive Induced Large Perovskite Grains for High Performance Inverted Solar Cells. *Sol. RRL* **2018**, *2*, 1800054.
(51) Lv, Y.; Zhang, H.; Wang, J.; Chen, L.; Bian, L.; An, Z.; Qian, Z.; Ren, G.; Wu, J.; Nüesch, F.; Huang, W. All-in-One Deposition to Synergistically Manipulate Perovskite Growth for High-Performance Solar Cell. *Research* **2020**, *2020*, 1−10.
(52) Schmager, R.; Fritz, B.; Hünig, R.; Ding, K.; Lemmer, U.; Richards, B. S.; Gomard, G.; Paetzold, U. W. Texture of the Viola Flower for Light Harvesting in Photovoltaics. *ACS Photonics* **2017**, *4*, 2687−2692.
(53) Roslizar, A.; Guttmann, M.; Lemmer, U.; Casas Soler, P.; Langenhorst, M.; Schneider, M.; Paetzold, U.; Huenig, R.; Fritz, B.; Richards, B.; Gomard, G. Towards Mass Fabrication of Hot Embossed Plant Surface Texture Replicas as Photovoltaic Cover Layers. In *Nanoengineering: Fabrication, Properties, Optics, and Devices*

XV; Sakdinawat, A. E., Attias, A.-J., Panchapakesan, B., Dobisz, E. A., Eds.; SPIE, 2018; p 17. DOI: 10.1117/12.2320555.
(54) Sutter, J.; Eisenhauer, D.; Wagner, P.; Morales Vilches, A. B.; Rech, B.; Stannowski, B.; Becker, C. Tailored Nanostructures for Light Management in Silicon Heterojunction Solar Cells. *Sol. RRL* **2020**, *4*, 2000484.
(55) Tockhorn, P.; Sutter, J.; Colom, R.; Kegelmann, L.; Al-Ashouri, A.; Roß, M.; Jäger, K.; Unold, T.; Burger, S.; Albrecht, S.; Becker, C. Improved Quantum Efficiency by Advanced Light Management in Nanotextured Solution-Processed Perovskite Solar Cells. *ACS Photonics* **2020**, *7*, 2589−2600.
(56) Chen, D.; Manley, P.; Tockhorn, P.; Eisenhauer, D.; Köppel, G.; Hammerschmidt, M.; Burger, S.; Albrecht, S.; Becker, C.; Jäger, K. Nanophotonic light management for perovskite-silicon tandem solar cells. *J. Photon. Energy* **2018**, *8*, 1.
(57) Dottermusch, S.; Schmager, R.; Klampaftis, E.; Paetel, S.; Kiowski, O.; Ding, K.; Richards, B. S.; Paetzold, U. W. Micro-cone textures for improved light in-coupling and retroreflection-inspired light trapping at the front surface of solar modules. *Prog. Photovoltaics Res. Appl.* **2019**, *27*, 3133.
(58) Song, Z.; Li, C.; Chen, L.; Yan, Y. Perovskite Solar Cells Go Bifacial-Mutual Benefits for Efficiency and Durability. *Adv. Mater.* **2022**, *34*, 2106805.
(59) Morales-Vilches, A. B.; Wang, E.-C.; Henschel, T.; Kubicki, M.; Cruz, A.; Janke, S.; Korte, L.; Schlatmann, R.; Stannowski, B. Improved Surface Passivation by Wet Texturing, Ozone-Based Cleaning, and Plasma-Enhanced Chemical Vapor Deposition Processes for High-Efficiency Silicon Heterojunction Solar Cells. *Phys. Status Solidi* **2020**, *217*, 1900518.
(60) Al-Ashouri, A.; Magomedov, A.; Roß, M.; Jošt, M.; Talaikis, M.; Chistiakova, G.; Bertram, T.; Márquez, J. A.; Köhnen, E.; Kasparavičius, E.; Levcenco, S.; Gil-Escrig, L.; Hages, C. J.; Schlatmann, R.; Rech, B.; Malinauskas, T.; Unold, T.; Kaufmann, C. A.; Korte, L.; Niaura, G.; Getautis, V.; Albrecht, S. Conformal Monolayer Contacts with Lossless Interfaces for Perovskite Single Junction and Monolithic Tandem Solar Cells. *Energy Environ. Sci.* **2019**, *12*, 3356−3369.
(61) Patel, J. B.; Wright, A. D.; Lohmann, K. B.; Peng, K.; Xia, C. Q.; Ball, J. M.; Noel, N. K.; Crothers, T. W.; Wong-Leung, J.; Snaith, H. J.; Herz, L. M.; Johnston, M. B. Light Absorption and Recycling in Hybrid Metal Halide Perovskite Photovoltaic Devices. *Adv. Energy Mater.* **2020**, *10*, 1903653.
(62) Li, Y.; Li, L.; Yerramilli, A. S.; Chen, Y.; Fang, D.; Shen, Y.; Alford, T. L. Enhanced Power Conversion Efficiency and Preferential Orientation of the MAPbI3 Perovskite Solar Cells by Introduction of Urea as Additive. *Org. Electron.* **2019**, *73*, 130−136.
(63) Merdasa, A.; Kiligaridis, A.; Rehermann, C.; Abdi-Jalebi, M.; Stöber, J.; Louis, B.; Gerhard, M.; Stranks, S. D.; Unger, E. L.; Scheblykin, I. G. Impact of Excess Lead Iodide on the Recombination Kinetics in Metal Halide Perovskites. *ACS Energy Lett.* **2019**, *4*, 1370−1378.
(64) Lehr, J.; Langenhorst, M.; Schmager, R.; Kirner, S.; Lemmer, U.; Richards, B. S.; Case, C.; Paetzold, U. W. Energy Yield Modelling of Perovskite/Silicon Two-Terminal Tandem PV Modules with Flat and Textured Interfaces. *Sustain. Energy Fuels* **2018**, *2*, 2754−2761.
(65) Phung, N.; Verheijen, M.; Todinova, A.; Datta, K.; Verhage, M.; Al-Ashouri, A.; Köbler, H.; Li, X.; Abate, A.; Albrecht, S.; Creatore, M. Enhanced Self-Assembled Monolayer Surface Coverage by ALD NiO in p-i-n Perovskite Solar Cells. *ACS Appl. Mater. Interfaces* **2022**, *14*, 2166−2176.
(66) Sun, J.; Shou, C.; Sun, J.; Wang, X.; Yang, Z.; Chen, Y.; Wu, J.; Yang, W.; Long, H.; Ying, Z.; Yang, X.; Sheng, J.; Yan, B.; Ye, J. NiO x -Seeded Self-Assembled Monolayers as Highly Hole-Selective Passivating Contacts for Efficient Inverted Perovskite Solar Cells. *Sol. RRL* **2021**, *5*, 2100663.
(67) Schmid, M.; Ludescher, D.; Giessen, H. Optical Properties of Photoresists for Femtosecond 3D Printing: Refractive Index, Extinction, Luminescence-Dose Dependence, Aging, Heat Treatment and Comparison between 1-Photon and 2-Photon Exposure. *Opt. Mater. Express* **2019**, *9*, 4564−4577.
(68) Almora, O.; Cabrera, C. I.; Garcia-Cerrillo, J.; Kirchartz, T.; Rau, U.; Brabec, C. J. Quantifying the Absorption Onset in the Quantum Efficiency of Emerging Photovoltaic Devices. *Adv. Energy Mater.* **2021**, *11*, 2100022.
(69) Sjerps-Koomen, E. A.; Alsema, E. A.; Turkenburg, W. C. A Simple Model for PV Module Reflection Losses under Field Conditions. *Sol. Energy* **1996**, *57*, 421−432.
(70) Martin, N.; Ruiz, J. M. Calculation of the PV Modules Angular Losses under Field Conditions by Means of an Analytical Model. *Sol. Energy Mater. Sol. Cells* **2001**, *70*, 25−38.